DE GRUYTER OPEN

***MINERALOGIA**, 48, No 1-4: 107-126 (2017)*
DOI: 10.1515/mipo-2017-0014
www.Mineralogia.pl

MINERALOGICAL SOCIETY OF POLAND
POLSKIE TOWARZYSTWO MINERALOGICZNE

Original paper

Halloysite composites with Fe_3O_4 particles: the effect of impregnation on the removal of aqueous Cd(II) and Pb(II)

Paulina Maziarz[1]*, Jakub Matusik[1]

[1] *AGH University of Science and Technology, Faculty of Geology, Geophysics and Environmental Protection, Department of Mineralogy, Petrography and Geochemistry, al. Mickiewicza 30, Krakow, 30 059, Poland*

** Corresponding author*

e-mail: pmaziarz@agh.edu.pl

Received: April 3, 2017
Received in revised form: August 29, 2017
Accepted: August 29, 2017
Available online: September 30, 2017

Abstract. In this study, halloysite-Fe_3O_4 composites were synthesized by a chemical-precipitation method to facilitate magnetic separation of the sorbents from aqueous solution. The research focused on the effect of Fe_3O_4 phase on the halloysite sorption properties. The X-ray diffraction (XRD) results confirmed successful deposition of Fe_3O_4 particles on a halloysite surface. They showed that the coating with Fe_3O_4 particles enhanced the halloysite adsorption affinity toward Cd(II) and Pb(II). The highest adsorption capacity was determined for the composites having 10% of the surface deposited with Fe_3O_4. In this case, the adsorption capacity for Cd(II) and Pb(II) was 33 and 112 $mmol \cdot kg^{-1}$, respectively. The point of zero charge (pH_{PZC}) and desorption results indicated that the removal mechanism of metals is mainly related to chemisorption involving reaction with hydroxyls of either halloysite or Fe_3O_4 phase. The ion exchange is of limited importance due to the low cation exchange capacity (CEC) of halloysite - Fe_3O_4 composites.

Key-words: Fe_3O_4 particles; Halloysite; Adsorption; Cd(II); Pb(II)

1. Introduction

The wide distribution and increased concentration levels of heavy metals in surface and ground water is mainly due to the discharge of industrial and agricultural wastes. These contaminants are particularly problematic and harmful due to their non-biodegradable character and tendency to accumulate in living organisms. This subsequently results in various disorders and diseases. Thus, environmental remediation has recently become one of the most common subjects of scientific discussion and research. Several methods are

known for water treatment including ion exchange, adsorption, coagulation and filtration, chemical precipitation, membrane processes, and reverse osmosis (Matlock et al. 2002; Ozaki et al. 2002; Blöcher et al. 2003; Dąbrowski et al. 2004; Unuabonah et al. 2008; Zhang and Hou 2008; Jiang et al. 2010; Motsi et al. 2011; Matusik, Wścisło 2014; Bajda et al. 2015; Koteja, Matusik 2015; Maziarz, Matusik 2016). Since among the various technologies developed for the removal of contaminants, the adsorption processes are the most effective, economical and commonly used, methods for adsorbent separation from the working medium need to be constantly developed.

In recent years, research on magnetic particles appears to be a dynamically developing branch of nanotechnology, and in particular regarding the field of their application in environmental remediation and catalysis. Apart from their nano-size, resulting in well-developed surface area and high adsorption capacity, their magnetic properties allow for their facile and effective separation by an outer magnetic field (Yantasee et al. 2007; Lunge et al. 2014; Kharissova et al. 2015; Mehta et al. 2015). Among magnetic particles, iron oxides such as magnetite (Fe_3O_4) and maghemite (γ-Fe_2O_3) are the most commonly used. However, one of the major problems with sole particles' application is connected with their agglomeration and chemical instability in acidic environments. Thus, in the last few decades research has focused on the synthesis of Fe_3O_4 particles combined with other commonly used adsorbents. As a result, the magnetic composites are prepared by a coating of a conventional adsorbent surface with Fe_3O_4 particles. This combination not only prevents agglomeration, but also allows to obtain promising magnetic composites. These can be easily separated from the working medium after being used by the application of an outer magnetic field. Due to these obvious benefits, knowledge concerning conventional adsorbents, especially widely available clay minerals coated with Fe_3O_4 particles, is constantly extending. To our best knowledge, composites consisting of magnetic Fe_3O_4 particles and clay minerals were successfully used as adsorbents of some inorganic metal cations (Oliveira et al. 2003; Hashemian et al. 2014), anions (Tian et al. 2016) and organic dyes (Oliveira et al. 2003; Zhang, Kong 2011; Duan et al. 2012).

In the present study, halloysite clay mineral was used as the support for Fe_3O_4 particles. Halloysite is an aluminum silicate belonging to the kaolin group of minerals. Its chemical formula is $Al_2Si_2O_5(OH)_4 \cdot 2H_2O$. Its structure is composed of 1:1 stacked layers, built from tetrahedral (Si) and octahedral (Al) sheets. The layers are linked through hydrogen bonding formed between the oxygen atoms of the tetrahedral sheet and the inner surface OH groups of the octahedral sheet (Joussein et al. 2005). Isomorphic substitution of the central ions in tetrahedral and octahedral sheets is very rare, resulting in an almost neutral surface charge (Joussein et al. 2005). The interest concerning halloysite has increased in recent years due to its possible utilization in nanotechnology applications, mainly connected with the halloysite nanotubular structure. To date, some halloysites were successfully used as supporting minerals for particles that exhibit catalytic properties, such as silver (Li et al. 2014), palladium (Fu et al. 2005) or titanium (Papoulis et al. 2010; Wang et al. 2011). Some research concerning the deposition of iron particles on halloysite surface (Xie et al. 2011; Duan et al. 2012; Amjadi et al. 2015) was also reported.

The objective of this study was to obtain and characterize magnetic composites, composed of halloysite and magnetite (Fe_3O_4) particles. In the study, a different loading of Fe_3O_4 on a halloysite surface was used. The affinity of the resulting halloysite-Fe_3O_4

composites for cationic heavy metals' species removal was investigated. For this purpose, adsorption equilibrium experiments for Pb(II) and Cd(II) ions were carried out. The possible mechanisms responsible for Pb(II) and Cd(II) adsorption were also identified.

2. Materials and methods

2.1. Materials

For the experiments, halloysite sample (H) was collected from the Polish deposit Dunino located in the Lower Silesia. The H sample was used in a powder form as received, without any further purification or grinding. The reagents were of analytical grade. During synthesis of the composites and adsorption experiments, re-distilled water was used.

2.2. Preparation of HFe_3O_4 composite

The impregnation of the H sample by Fe_3O_4 particles was performed by a chemical precipitation method (Xie et al. 2011; Duan et al. 2012). Firstly, the suspension of H sample (5.0 g) in an aqueous solution (200 ml) was prepared and vigorously stirred. In order to obtain the Fe_3O_4 particles, the solution of iron precursors consisting of ferric chloride hexahydrate ($FeCl_3 \cdot 6H_2O$) and ferrous sulfate heptahydrate ($FeSO_4 \cdot 7H_2O$) was dropwise added to the H sample suspension. The stoichiometric ratio of Fe(III):Fe(II) in the solution was set to 2:1. The pH of the obtained mixture was constantly controlled, in the range of 9 – 10 using 4 $mol \cdot L^{-1}$ NaOH solution, to initiate the chemical precipitation of the iron oxides. The NaOH solution was added until the pH reached an equilibrium, which indicated the completion of the reaction. The final black suspension was washed 4 times with re-distilled water and dried at 60°C for 24h. The mass ratio of Fe_3O_4 to the H was set to 10% (HFe10), 25% (HFe25), and 50% (HFe50). The pure Fe_3O_4 phase was synthesized using the above procedure for comparison. In order to obtain such mass ratios, the appropriate amounts of ferric and ferrous reagents were used (Table 1). Additionally, the HFe10, HFe25 and Fe_3O_4 samples were thermally treated at 400°C for 3h. The obtained calcined samples were marked as HFe10K, HFe25K, and Fe_3O_4K.

2.3. Characterization methods

The crystalline phases in the HFe_3O_4 composites were characterized with X-ray diffraction (XRD). The XRD patterns of the powdered samples were recorded in the range of 2–73°2θ with step equal to 0.05º2θ, using a RIGAKU Miniflex 600 diffractometer with CuKα (λ=1.5418 Å) radiation. The quantitative elemental analysis was carried out by a WD-XRF ZSX Primus II Rigaku spectrometer. The values reported by the XRF were calculated by the SQX calculation program. The FTIR spectra of the samples, prepared as KBr pellets (3 mg sample per 197 mg KBr), were recorded using a Nicolet 6700 spectrometer (Thermo Scientific). For each measurement, 64 scans were collected in the range of 4000 – 400 cm^{-1} with a resolution of 4 cm^{-1}.

TABLE 1

List of reagents used during synthesis of HFe_3O_4 composites.

Sample	$FeCl_3 \cdot 6H_2O$ [g]	$FeSO_4 \cdot 9H_2O$ [g]	Fe_3O_4* [g]	H [g]
HFe10	1.18	0.60	0.5	
HFe25	2.91	1.50	1.25	5.0
HFe50	5.82	3.00	2.5	
Fe_3O_4	11.64	6.00	5.0	-

*The theoretical calculated amount of Fe_3O_4 formed during the synthesis.

The point of zero charge (pH_{PZC}) was determined using 0.05 mol·L^{-1} aqueous KOH solution for preparing suspensions of the materials with three different mass ratios (1 g·L^{-1}, 2 g·L^{-1}, and 4 g·L^{-1}). The suspensions were equilibrated for 24h to provide optimum dispersion and reach an equilibrium pH. The blank 0.05 mol KOH solution and suspensions were titrated with 0.05 mol·L^{-1} HNO_3. The pH value was recorded after each addition of 0.05 ml HNO_3. The pH_{PZC} value was evaluated, as the intersection of the titration curves for the three suspension mass ratios and the blank solution.

The cation exchange capacity (CEC) was measured by hexaamminecobalt(II) chloride as a probing molecule. The measurements were done in duplicate. In the experiment, 100 mg of each material was mixed with 5 ml of 2 g·L^{-1} hexaamminecobalt(II) chloride (solid:liquid ratio – 20 g·L^{-1}). The suspensions were shaken for 1h. The final concentration of hexaamminecobalt(II) chloride in supernatant solution was measured using UV-Vis spectroscopy at 470 nm wavelength.

2.4. Equilibrium adsorption experiments

The adsorption properties were determined for the H, HFe10, HFe25, and their calcined derivatives. The adsorption equilibrium experiments were conducted in single element aqueous solutions of Cd(II) and Pb(II) at initial concentrations (C_{in}) the range of 0.1-25.0 mmol·L^{-1}. The stock solutions were prepared by dissolving $Cd(NO_3)_2 \cdot 4H_2O$ and $Pb(NO_3)_2$, respectively. The equilibrium isotherms were carried out in duplicate at room temperature. The initial pH (pH_{in}) of the solutions was set to 5.0 ± 0.2, which was recommended as optimal in Cd(II) and Pb(II) adsorption processes (Ebrahim et al. 2015; Hosseinzadeh et al. 2016; Rajput et al. 2016). The pH was adjusted by using 0.1 mol HNO_3 and 0.1 mol NaOH solutions. The solid:liquid ratio was equal to 20 g·L^{-1}. After 24h of shaking, the mixtures were centrifuged at 14 000 rpm for 5 min. The Cd(II) and Pb(II) concentrations in the supernatant solutions were measured using Atomic Absorption Spectroscopy (AAS).

2.5. Desorption experiment

The desorption experiment was conducted for 5 mmol·L^{-1} concentration of Cd(II) and Pb(II). Firstly, the adsorption of cations was carried out according to the procedure

described above. After adsorption, the samples were washed several times with re-distilled water to remove the excess of adsorbates not adsorbed by the composites. Then, before the desorption experiment the samples were dried at 60°C for 24h and weighed. The 1 mol·L^{-1} CH_3COONH_4 (pH = 7.0) was used as a desorbing reagent, with the solid:liquid ratio ~100 mg : 5 ml (20 g·L^{-1}) (Rzepa et al. 2009). The desorption was carried out in two steps: for 1h and 24h of contact time. The concentration of metals in solutions in the desorption experiment was measured using Atomic Absorption Spectroscopy.

2.6. Equilibrium adsorption models

In order to describe the Cd(II) and Pb(II) adsorption on the resulting composites and investigate the mechanisms of adsorption, the experimental equilibrium isotherms were fitted to Langmuir, Freundlich and Dubinin-Radushkevich models. The Langmuir model assumed the monolayer adsorption and no interactions between the adsorbed molecules on the homogenous surface of the adsorbent with a finite number of active sites (Langmuir 1916). It is usually applied for chemisorption. The Freundlich model allows multilayer adsorption, which is characterized by the heterogeneous distribution of energy. The energy of adsorbate binding depends on whether the adjacent active sites are already occupied (Freundlich 1906). The Dubinin–Radushkevich equation is generally applied to express the adsorption energy onto a heterogeneous surface. It also allows to define the character of the adsorption mechanism (Dubinin 1960). The value of the mean free energy of adsorption E_{DR} < 8 kJ·mol^{-1} corresponds to the non-specific physisorption, the E_{DR} in the range of 8–16 kJ·mol^{-1} corresponds to an ion-exchange reaction, while E_{DR} > 16 kJ·mol^{-1} can be attributed to chemisorption (Elkamash et al. 2005). The Langmuir (1), Freundlich (2) and Dubinin–Radushkevich (3) equations are given as:

$$q_{eq} = \frac{K_L q_m C_{eq}}{1+K_L C_{eq}} \quad (1)$$

$$q_{eq} = K_F C_{eq}^{\frac{1}{n}} \quad (2)$$

$$q_{eq} = q_{DR} e^{(-K_{DR}\varepsilon^2)} \quad (3)$$

where q_{eq} – sorption capacity at equilibrium (mmol·kg^{-1}); C_{eq} – equilibrium concentration of adsorbate (mmol·L^{-1}); K_L – Langmuir adsorption constant (L·$mmol^{-1}$), which relates to the free energy and affinity of the adsorption; q_m – maximum adsorption capacity (mmol·kg^{-1}); K_F – Freundlich adsorption capacity (mmol·kg^{-1}); n – Freundlich dimensionless constant, the degree of the adsorption dependence at equilibrium concentration; q_{DR} – Dubinin–Radushkevich adsorption capacity (mmol·kg^{-1}); K_{DR} – Dubinin–Radushkevich adsorption constant ($mmol^2/J^2$); e – Polanyi potential: $e = RT\ln(1 + 1/C_{eq})$.

Based on the Dubinin–Radushkevich equation, the mean free energy of adsorption $E_{DR}=(-2K_{DR})^{-1/2}$ was also calculated.

3. Results and discussion

3.1. XRD results

The XRD patterns of the H and HFe_3O_4 composites are shown in Figure 1. The starting H sample used in the study revealed a basal reflection at 7.2 Å, which is typical for dehydrated halloysite. In the XRD patterns of the HFe50 and HFe25, new peaks at 2.95 Å, 2.52 Å, 2.08 Å, 1.70 Å, 1.61 Å, and 1.48 Å can be attributed to the presence of Fe_3O_4. This indicated the success of the Fe_3O_4 synthesis on the H sample surface. In the case of the HFe10, the Fe_3O_4 peaks are not evident. However, in comparison to the H sample, changes in the intensity and clear broadening of the peaks in positions characteristic to Fe_3O_4 can be observed. This suggested that a minor amount of Fe_3O_4 was also formed in this case. The halloysite peaks on all XRD patterns were unaltered, which confirms that iron particles

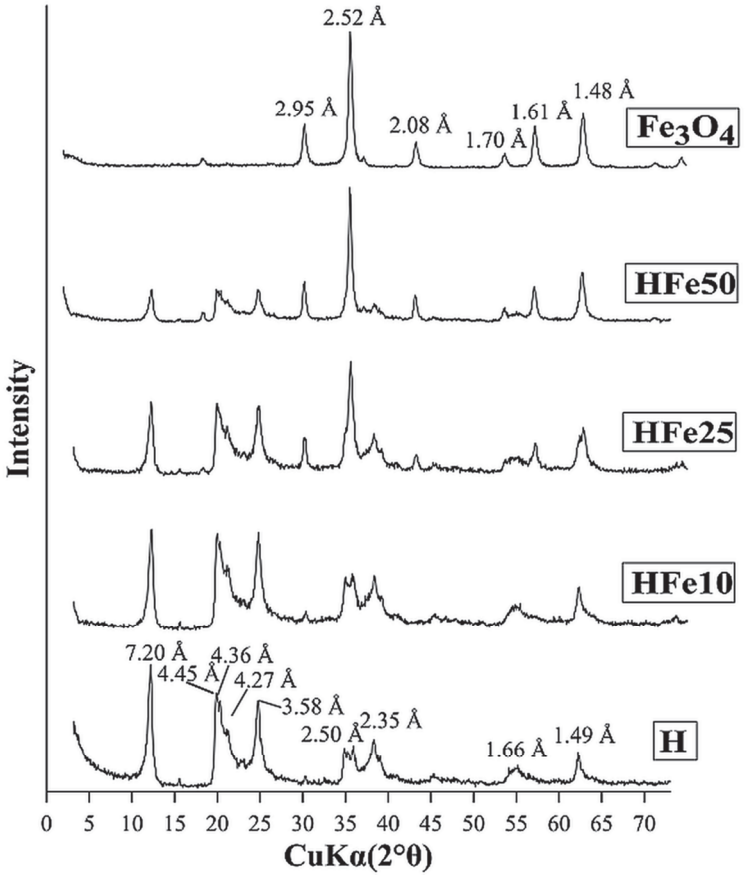

Fig. 1. The XRD patterns of H, HFe_3O_4 composites (HFe10, HFe25, and HFe50), and Fe_3O_4 phase (Fe_3O_4).

were exclusively deposited on the mineral surface. The intercalation of the H sample did not take place. After calcination, the characteristic reflections of halloysite and Fe_3O_4 phase were still present, indicating their structural stability in the applied conditions (Fig. 2). In turn, the relative decrease of 7.2 Å peak intensity as compared to the pure halloysite resulted from a decrease in the layered stacking order.

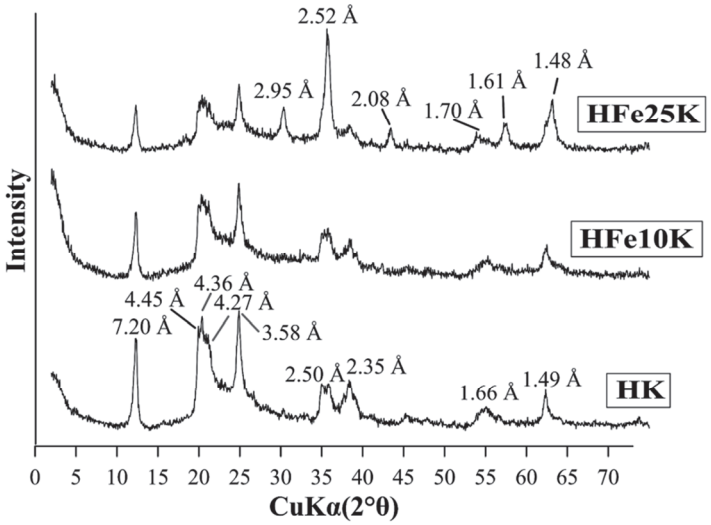

Fig. 2. The XRD patterns of HK, HFe10K, and HFe25K.

3.2. FTIR results

Figure 3 shows the FTIR spectra of the H, HFe10, HFe25, HFe50, and Fe_3O_4. The spectra of all samples revealed bands characteristic for the kaolin group of minerals. This confirmed that the original structure of the H sample was not altered during coating with Fe_3O_4. The adsorption bands at 3800 – 3600 cm^{-1} were ascribed to four different stretching vibration modes of the OH groups. The bands at 3695 cm^{-1}, 3670 cm^{-1}, and 3655 cm^{-1} can be attributed to inner-surface hydroxyls, while the band at 3620 cm^{-1} can be ascribed to inner hydroxyls (Rouxhet et al. 1977; Theng et al. 1982). In the region of 1500 – 400 cm^{-1}, intense bands attributed to vibrations within the aluminosilicate framework were observed. The bands due to Si-O stretching were present at 1100 – 1000 cm^{-1}, whereas Si–O–Si and Al–O–Si bending vibrations were observed at 550 – 400 cm^{-1}. The sharp band at 910 cm^{-1} can be attributed to the bending vibration of Al–OH. The Al-O-Si inner surface vibrations were connected with bands at 780 cm^{-1} and 750 cm^{-1}. Moreover, after coating with Fe_3O_4 the appearance of a new peak at 630 cm^{-1} and the broadening of a band at 540 cm^{-1} can be attributed to vibration within the Fe_3O_4. These bands were attributed to Fe-O symmetric stretching vibrations in crystalline lattice (Silva et al. 2013; Magnacca et al. 2014; Ghasemi et al. 2017; Karimzadeh et al. 2017). Moreover, the positions of these bands are characteristic to magnetite and maghemite (Fu et al. 2008; Wang et al. 2010; Iyengar et al. 2014). The adsorption bands at 3430 cm^{-1} and 1630 cm^{-1} in the Fe_3O_4 spectrum correspond

to the stretching and bending vibrations of the water molecules, which most likely were adsorbed on the surface of the Fe_3O_4 particles and halloysite.

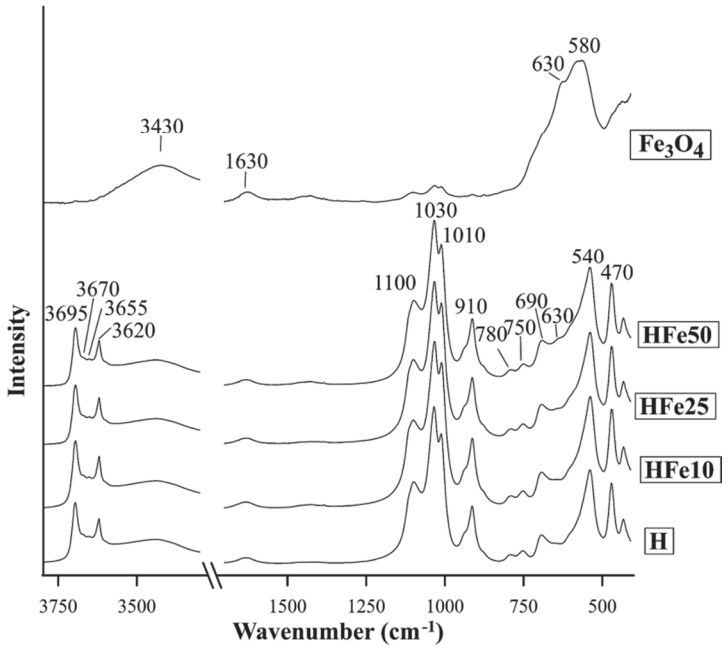

Fig. 3 The FTIR spectra of H, HFe10, HFe25, HFe50, and Fe_3O_4. The spectra of H, HFe10, HFe25, and HFe50 were normalized to the Si–O vibration band at 1030 cm^{-1}.

After thermal treatment, the relative intensities of the OH groups' bands, at 3700 - 3600 cm^{-1}, showed minor changes in comparison to the pure H sample (Fig. 4). This may indicate partial dehydroxylation of the H and HFe_3O_4 composites. The decrease of band intensities at 910 cm^{-1} was observed, which was also related to the dehydroxylation process. The intensity of Al-O-Si bending band at 540 cm^{-1} was weaker for the calcined samples, indicating the partial destruction of Al-O-Si bonds in the H sample. Additionally, the originally sharp band at 1100 cm^{-1} partially disappeared at the spectra of the calcined samples. The spectra of the thermally treated samples also revealed a band at 630 cm^{-1}, attributed to the Fe-O vibrations of Fe_3O_4. The FTIR spectra of Fe_3O_4K did not reveal any band attributed to OH vibration. Moreover, the shift in Fe-O vibration bands indicated partial transformation into hematite (Rendon, Serna 1981; Rodulfo-Baechler et al. 2004). However, after calcination a band at 630cm-1 characteristic to Fe_3O_4 was present in the FTIR spectra of the HFe_3O_4 composites. This suggested that transformation into hematite is hindered and does not take place when Fe_3O_4 particles are dispersed and deposited on the H surface, in contrast to bulk Fe_3O_4.

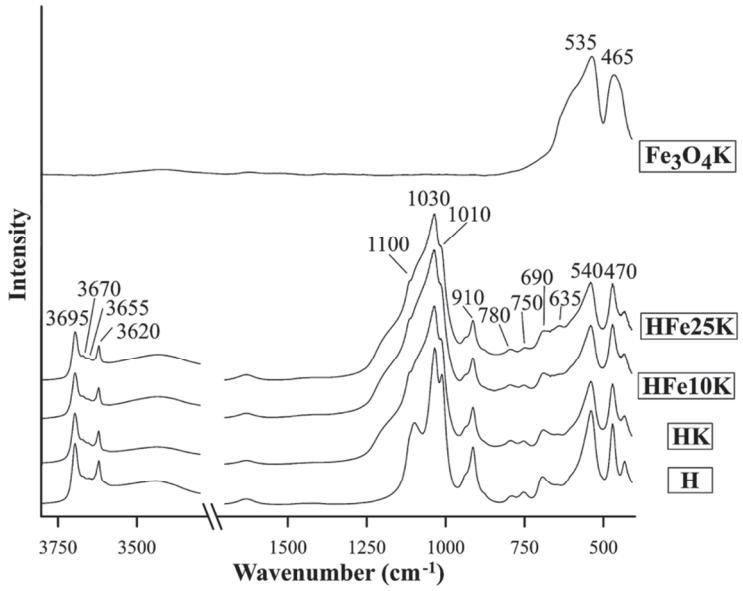

Fig. 4 The FTIR spectra of H, HK, HFe10K, HFe25K, and Fe_3O_4K. The spectra of H, HK, HFe10K, and HFe25K were normalized to the Si–O vibration band at 1030 cm^{-1}.

3.3. XRF results

The results of the elemental analysis for the H and HFe_3O_4 composites are shown in Table 2. As expected, the content of iron (Fe_2O_3) in the HFe_3O_4 composites was the highest for the HFe50 and lowest for the HFe10. The content of the other elements was not changed significantly. After coating with Fe_3O_4, the Al:Si molar ratio was unaltered and equal to ~1:1. The content of Fe and Ti in the H sample is connected with the presence of magnetite (Fe_3O_4), ilmenite ($FeTiO_2$), and maghemite (γ-Fe_2O_3), the presence of which was confirmed in previous studies (Matusik 2010).

Taking into account the iron content for the HFe_3O_4 composites and the natural H sample, the mass ratio of Fe_3O_4, which was formed during the synthesis to the H sample, was calculated (Table 2). The XRF results indicated that the content of Fe_3O_4 increased as follows: HFe10<HFe25<HFe50. However, the content of Fe_3O_4 for the HFe50 was 33.7%, which was much lower than 50%. This indicated that the synthesis was not as effective as in the case of the other samples. The comparison of the obtained results revealed that the effectiveness of Fe_3O_4 formation decreased with increasing Fe(III) and Fe(II) content in the solution during the synthesis procedure. Moreover, when the Fe_3O_4 content was high, the excess of iron particles weakly bonded to the kaolinite surface was probably removed during washing after synthesis.

TABLE 2

The chemical composition of H and the HFe_3O_4 composites in % mass and the content of Fe_3O_4 formed during synthesis for the HFe_3O_4 composites.

	HFe10	HFe25	HFe50	H
SO_3	0.1085	0.1314	0.1035	0.4022
P_2O_5	0.52	0.51	0.43	0.38
TiO_2	1.54	1.48	1.3	1.3
CeO_2	0.1	0.06	0.07	0.08
ZrO_2	0.11	0.12	0.04	0.1
SiO_2	44.75	42.22	36.33	30.32
Fe_2O_3	10.65	16.14	27.82	38.88
Al_2O_3	41.41	38.64	33.04	28.06
Cr_2O_3	0.04	0.03	0.05	0.04
Co_2O_3	0.02	0.02	0.04	0.05
Y_2O_3	0.01	0.01	0.01	0.01
MgO	0.07	0.05	0.06	0.08
CaO	0.15	0.13	0.13	0.13
MnO	0.04	0.04	0.05	0.07
NiO	0.04	0.04	0.04	0.04
CuO	0.01	0.01	0.01	0.01
ZnO	0.01	0.01	0.01	0.09
SrO	0.04	0.04	0.04	0.04
BaO	0.15	0.11	0.1	0.12
Na_2O	0.17	0.12	0.21	0.05
K_2O	0.04	0.12	0.11	0.02
Cl	0.01	0.01	0.01	0.02
Al/Si molar ratio	1.13	1.12	1.14	1.25
Mass ratio of Fe_3O_4 to H [%]	11.7	23.0	33.7	-

3.4. The adsorption experiments' results

The adsorption isotherms of the uncalcined and calcined samples for Cd(II) and Pb(II) are shown in Figure 5 and Figure 6, respectively. For all the adsorbents, the equilibrium adsorption capacity (represented by the "plateau" of the isotherm) was reached for the range of concentrations set in the experiments. The sorption capacity was calculated as the average of the last two experimental points on the isotherms.

The adsorption increased with the increasing initial Cd(II) concentration, although the exception was in the case of 25 $mmol \cdot L^{-1}$ initial concentration, where a slight decrease of Cd(II) adsorption was observed (Fig. 5). The results of Cd(II) adsorption indicated that the H sample derivatives coated with Fe_3O_4 had higher adsorption affinity toward Cd(II) than the raw H sample. For the thermally treated HFe_3O_4 composites, the observed adsorption capacities were similar to those for the H sample. The most promising adsorption capacity was obtained for the HFe10 sample and was equal to 32 $mmol \cdot kg^{-1}$. It was noticed that for

the HFe25 sample, the adsorption capacity was also higher than for the H sample, but lower than for the HFe10 sample. The results also showed that the heat treatment of the HFe10 and HFe25 decreased their adsorption properties toward Cd(II). The resulting adsorption isotherms follow the Langmuir equilibrium equation with the correlation coefficient $R^2 > 0.97$ (Table 3). The data calculated with the Langmuir equation (q_m) were in agreement with the experimental adsorption capacity.

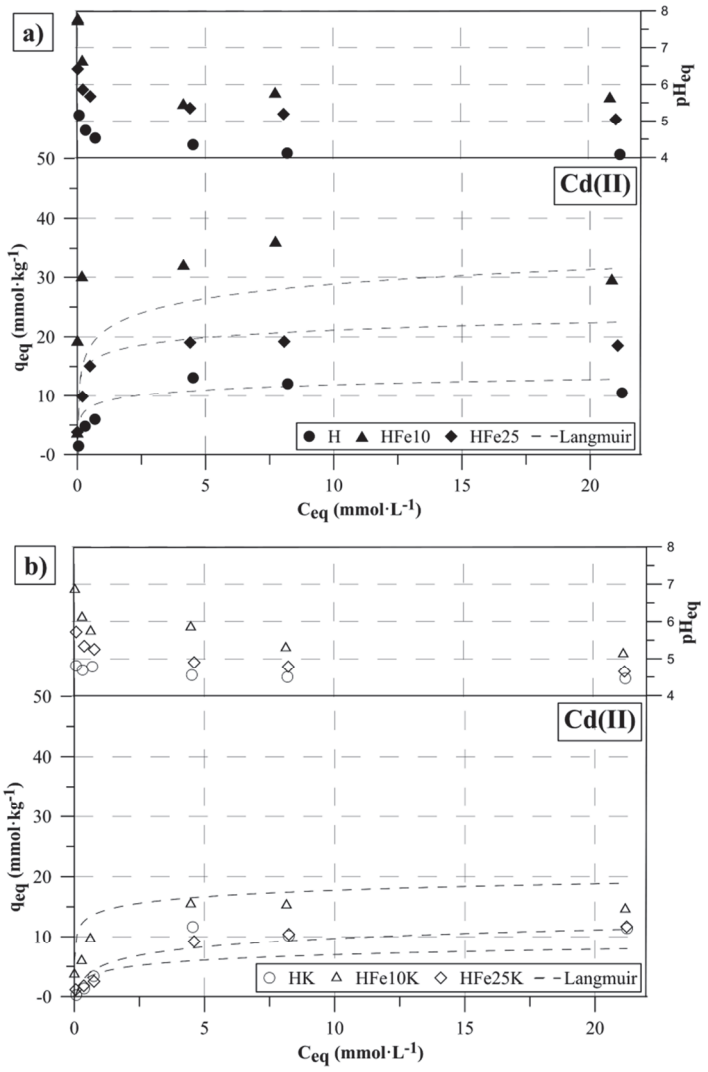

Fig. 5. The adsorption isotherms of a) uncalcined samples (H, HFe10, and HFe25) and b) calcined samples (HK, HFe10K, and HFe25K) for Cd(II) (contact time 24 h, pH_{in}=5.0, T=22°C).

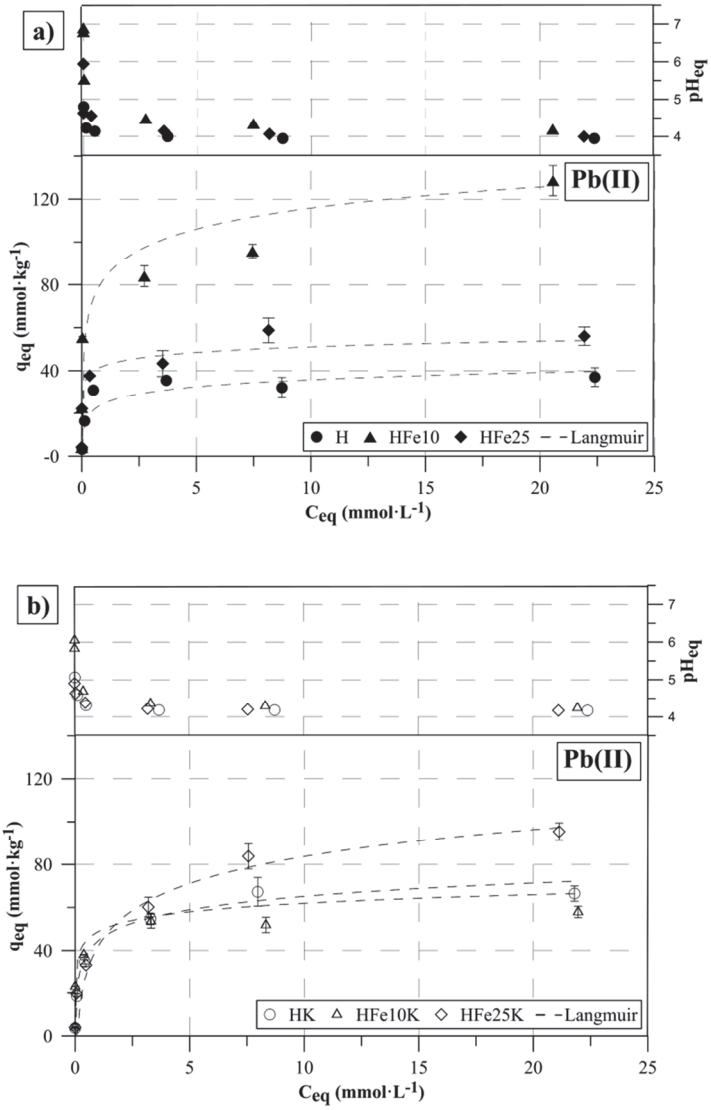

Fig. 6. The adsorption isotherms of a) uncalcined samples (H, HFe10, and HFe25) and b) calcined samples (HK, HFe10K, and HFe25K) for Pb(II) (contact time 24 h, pH_{in}=5.0, T=22°C).

TABLE 3

Parameters calculated from the Langmuir, Freundlich and Dubinin–Radushkevich models.

Ion	Sample	Langmuir			Freundlich			Dubinin-Radushkevish		
		q_m	K_L	R^2	1/n	K_F	R^2	q_e	E	R^2
		$mmol \cdot kg^{-1}$	$L \cdot mmol^{-1}$	-	-	$mmol \cdot kg^{-1}$	-	$mmol \cdot kg^{-1}$	$kJ \cdot mol^{-1}$	-
Cd(II)	H	10.8	103.3	0.9934	0.34	357.9	0.8461	14.7	10.2	0.9294
	HK	7.4	1.2	0.9818	0.86	958.4	0.8882	21.3	7.7	0.9796
	HFe10	30.6	2.4	0.9760	0.16	940.3	0.6068	34.2	28.9	0.8255
	HFe10K	14.8	225.7	0.9973	0.19	18.8	0.8808	15.7	16.2	0.8727
	HFe25	18.6	53.6	0.9996	0.16	23.3	0.9350	19.9	18.3	0.9704
	HFe25K	11.3	0.5	0.9765	0.43	165.5	0.9541	11.6	9.6	0.9245
Pb(II)	H	36.4	3.6	0.9966	0.27	50.5	0.8235	47.5	12.0	0.8684
	HK	66.6	3.2	0.9990	0.35	202.5	0.9147	81.4	11.5	0.9768
	HFe10	124.2	1.5	0.9828	0.26	145.1	0.7609	131.2	17.7	0.8056
	HFe10K	58.4	85.5	0.9988	0.21	76.7	0.8113	67.9	16.2	0.8698
	HFe25	56.2	4.9	0.9970	0.16	64.4	0.9785	53.7	22.4	0.9915
	HFe25K	93.3	1.2	0.9922	0.32	107.9	0.9901	86.1	12.9	0.9913

The coating of the H with Fe_3O_4 positively affected the adsorption capacity of the starting H sample for Pb(II) (Fig. 6). The adsorption increased with an increasing concentration of Pb(II) in the solution. The highest adsorption capacity was obtained, similarly to the case of Cd(II), for the HFe10 sample. It is worth noting that this adsorption capacity was equal to 112 $mmol \cdot kg^{-1}$, which was about 3-fold higher than in the case of the H sample. The least effective sorption of Pb(II) was observed for the H and the HFe25, where the adsorption capacity was equal to 35 $mmol \cdot kg^{-1}$ and 57 $mmol \cdot kg^{-1}$, respectively. The results showed that the calcination positively affected the adsorption capacity of the starting H and HFe25 samples. The opposite effect was obtained for the HFe10 sample, where the heat treatment caused a decrease of adsorption capacity. The experimental isotherms were fitted to the Langmuir model, with high correlation coefficient (R^2>0.98) (Table 3). The maximum adsorption capacity calculated from the Langmuir model was in good agreement with the experimental data. For the HFe25 and the HFe25K, the experimental data of Pb(II) adsorption were also fitted to the Dubinin–Radushkevish model, with high correlation coefficient ($R^2 > 0.99$). However, the calculated maximum adsorption from the Langmuir model (q_m) was closer to the experimental data.

The removal efficiency diagrams for the H and two HFe_3O_4 composites with the highest adsorption capacity for Cd(II) and Pb(II) are shown in Figure 7. Generally, it can be observed that the removal efficiency decreased with increasing C_{in}. The most significant changes were observed for Cd(II) adsorption (Fig. 7a). The highest efficiency for C_{in} concentrations below 1 $mmol \cdot L^{-1}$ was represented by the HFe10 sample. It is worth highlighting that for C_{in} ~0.1 $mmol \cdot L^{-1}$ and ~0.5$mmol \cdot L^{-1}$ the efficiency for the HFe10 was almost 100%. In the case of Pb(II) adsorption, the removal efficiency changes were not as significant as those for Cd(II) (Fig. 7b). The highest percentage removal was determined for the HFe10. Moreover, the results indicated that for C_{in} in the range of 0.1 – 1.0 $mmol \cdot L^{-1}$, almost 100% of the Pb(II) ions were removed from the solution. These results revealed that the HFe10 composite can be used as a very effective adsorbent at low Cd(II) and Pb(II) concentrations.

3.5. Desorption experiment results

Previous studies have shown that 1$mol \cdot L^{-1}$ CH_3COONH_4 has the ability to desorb ion-exchanged species, while chemically adsorbed complexes remained unaffected (Rzepa et al. 2009). The result of the experiment for the H sample revealed that after 2 desorption steps, 65% of Cd(II) and 45% of Pb(II) was removed (Fig. 8). These result were in agreement with previously reported studies (Maziarz, Matusik 2016). After coating the halloysite surface with Fe_3O_4 and applying heat treatment, the desorption decreased. In the case of Cd(II) and Pb(II) desorption did not exceed 30% and 20%, respectively. In the second step, the percentage of desorbed cations was lower than in step 1. This revealed that the vast majority of ion-exchanged cations was removed in the first 1h of desorption. Most of the Cd(II) and Pb(II) was not desorbed from the HFe_3O_4 composites after the second step of desorption.

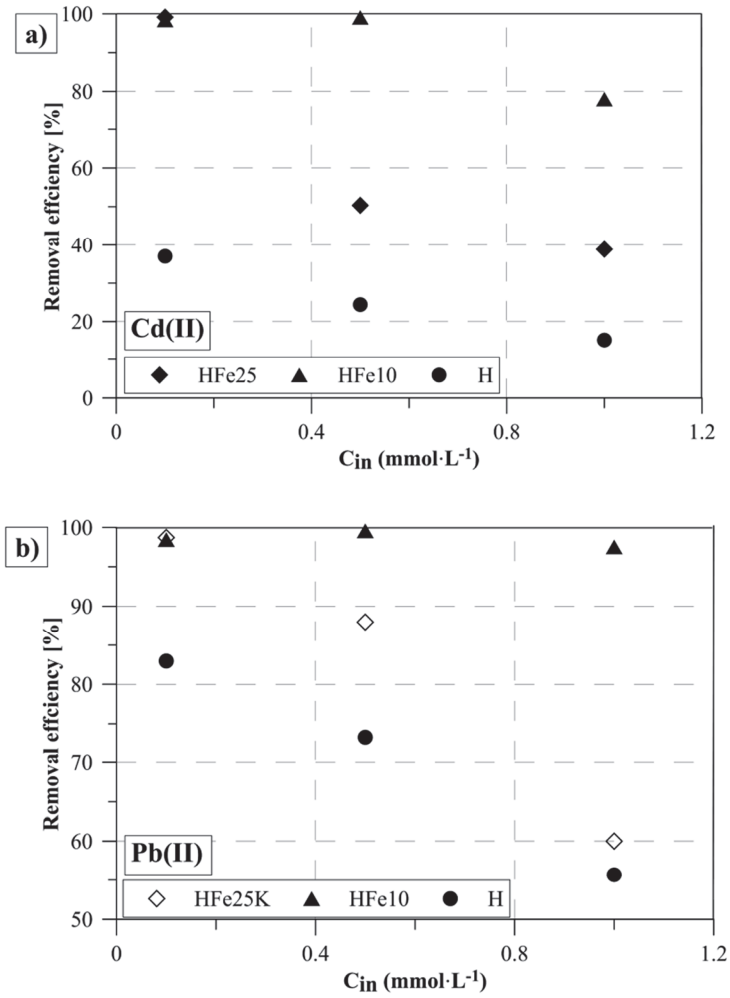

Fig. 7. The removal efficiency for C_{in} in the range of 0.1 – 5.0mmol·L^{-1} of a) Cd(II) for H, HFe10, and HFe25, and b) Pb(II) for H, HFe10, and HFe25K (contact time 24 h, pH_{in}=5.0, T=22°C).

3.6. The mechanisms and factors influencing adsorption

The higher adsorption capacity of Pb(II) as compared to Cd(II) can be related to differences in their chemical properties. This mainly involves the hydrolysis constant and ionic radius. Literature on Cd(II) and Pb(II) ionic species distribution versus pH reports that the dominant forms at pH < 6.0 are Cd^{2+} and Pb^{2+}, $Pb(OH)^{+}$, respectively which is strictly connected with the metals' hydrolysis constants (Smičiklas et al. 2000; Xu et al. 2008). Previous studies indicated that the adsorption of Cd(II) by the H sample occurs mainly through ion exchange, while in the case of Pb(II) removal both ion exchange and surface complexation can take place (Matusik 2016; Maziarz, Matusik 2016). This may be evidence for lower adsorption in the case of Cd(II). Additionally, the adsorption of Cd(II)

and Pb(II) can be interpreted in terms of their hydrated ionic radii, which are equal to 4.26 Å and 4.01 Å, respectively (Nightingale 1959; Wang et al. 2015). With the increase of hydrated ionic radius, the adsorption is less efficient because of the weaker interaction with the hydroxyls of deposited iron particles.

The results indicated that the coating with Fe_3O_4 can positively influence the adsorption capacity of the H sample. The CEC, pH_{PZC} (Table 4), and desorption results (Fig. 8) indicated that adsorption by introduced Fe_3O_4 particles is represented by chemical reactions, most likely surface complexation. The ion-exchange mechanism involving electrostatic interactions is of limited importance. This is due to the very low CEC of the H sample. Moreover, the deposition of Fe_3O_4 particles did not influence significantly the cation exchange properties of the resulting HFe_3O_4 composites (Table 4). A slight decrease of CEC was observed for the calcined samples, which can be explained by a partial loss of exchangeable cations during thermal treatment.

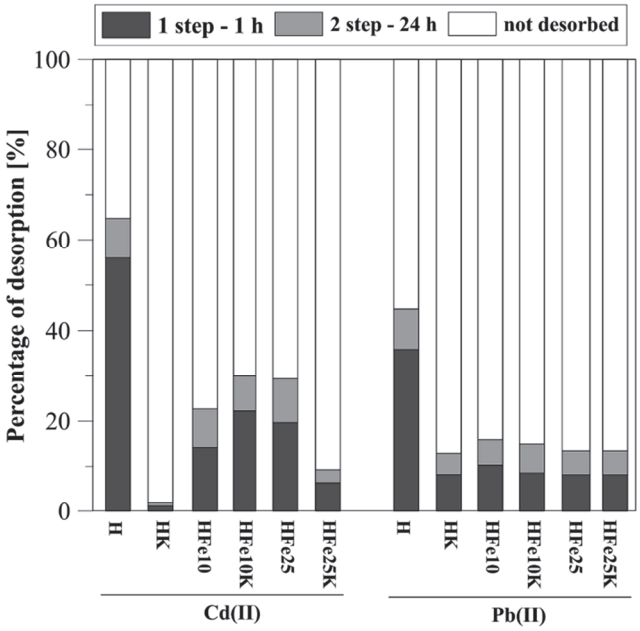

Fig. 8 The desorption results after 1 h and 24 h of contact time with desorbing agent (1 $mol \cdot L^{-1}$ CH_3COONH_4, pH=7.0) for Cd(II) and Pb(II).

The formation of chemically adsorbed species was mainly attested through desorption experiments. For both the Cd(II) and Pb(II), the percentage of non-desorbed metals was higher than 70% and 80%, respectively. The Pb(II) and Cd(II) uptake can proceed through the replacement of surface protons in Fe-OH groups (Kumari et al. 2015; Bagbi et al. 2016). This interaction can result in the formation of monodentate and bidentate complexes (Fig. 9). The formation of these complexes was in agreement with the pH changes. The pH_{eq} decreased during the adsorption as the surface OH groups underwent deprotonation, thus creating additional active sites for Cd(II) and Pb(II) adsorption.

TABLE 4

The CEC and pH_{PZC} results for the studied materials.

Sample	CEC [meq per 100 g]	pH_{PZC} [-]
H	5.3 ± 0.0	2.20± 0.02
HK	4.5 ± 0.1	4.38 ± 0.02
HFe10	5.1 ± 0.1	2.89 ± 0.02
HFe10K	4.2 ± 0.1	6.0 ± 0.02
HFe25	4.8 ± 0.2	3.02 ± 0.02
HFe25K	2.4 ± 0.2	4.01 ± 0.02

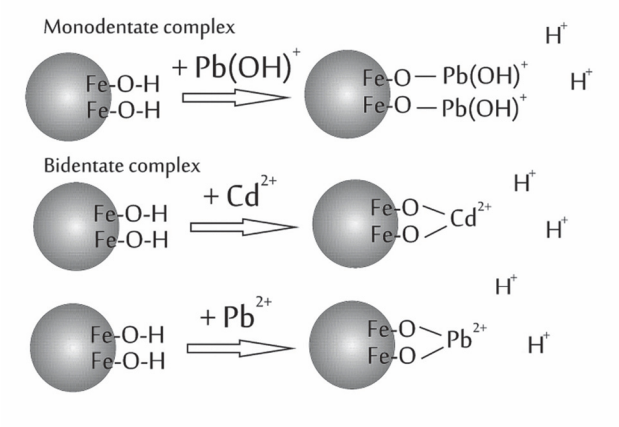

Fig. 9. Schematic diagram of possible Cd(II) and Pb(II) adsorption mechanism.

A decrease in adsorption capacity of the calcined HFe_3O_4 composites was observed. It was connected with the partial loss of Fe_3O_4 surface OH groups, confirmed by the FTIR (Fig. 4). The pH_{PZC} measured for the HFe_3O_4 composites revealed that for the pH_{in}=5.0, the surface of uncalcined composites was negatively charged and so favors the adsorption of positively charged species. After heat treatment, the composites showed varied surface-charge properties. The pH_{PZC} value revealed that for the pH_{in}=5.0, the surface of HFe10K was positively charged, which hampers the adsorption of cations, while the HFe25K surface was negatively charged, thus facilitating the removal of cations.

The mean free energy of adsorption E_{DR} for the HFe_3O_4 composites calculated from the Dubinin–Radushkevish equation was found to be >16 $kJ \cdot mol^{-1}$, with the exception of HFe25K, for which the E_{DR} was found to be <8 $kJ \cdot mol^{-1}$ (Table 3). This also indicated that chemisorption was the dominating mechanism in Cd(II) and Pb(II) adsorption by the HFe_3O_4 composites. In the case of HFe25K, the physisorption processes can be related to its negatively charged surface for the pH_{in}=5.0 and the partial loss of surface OH groups.

It is worth mentioning that the mass ratio of Fe_3O_4 to H played a significant role concerning the efficiency of metals' removal. The analyses indicated that 25% of the Fe_3O_4 resulted in the agglomeration of Fe_3O_4 particles, which negatively affected the adsorption.

4. Conclusions

The characterization results indicated that the Fe_3O_4 particles were successfully synthesized by chemical precipitation on the H sample surface. The adsorption results showed that coating the H surface with Fe_3O_4 positively influences its adsorption capacity. However, the mass ratio of Fe_3O_4 to H significantly affects the adsorption properties. For both Cd(II) and Pb(II), the highest adsorption capacity was observed for the HFe10 sample, and was equal to 32 $mmol \cdot kg^{-1}$ and 112 $mmol \cdot kg^{-1}$, respectively. The CEC, pH_{PZC} and desorption results indicated that the adsorption mechanism of Cd(II) and Pb(II) is more likely to be attributed to chemisorption involving adsorbed ions and the Fe_3O_4 particles' surface. The equilibrium adsorption isotherms followed the Langmuir model with a very high correlation coefficient and good correlation of the experimental results to the calculated Langmuir adsorption capacity. The overall results indicated that the HFe_3O_4 composites can be considered as promising adsorbents for cations removal, especially at low concentrations that are commonly found in the environment and industrial wastewaters.

Acknowledgments. This project was supported by the National Science Centre, Poland, under a research project awarded by Decision No. 2016/21/N/ST10/00390.

5. References

Amjadi, M., Samadi, A., & Manzoori, J. L. (2015). A composite prepared from halloysite nanotubes and magnetite (Fe_3O_4) as a new magnetic sorbent for the preconcentration of cadmium(II) prior to its determination by flame atomic absorption spectrometry. *Microchimica Acta*. *182*(9-10), 1627-1633. DOI:10.1007/s00604-015-1491-y.

Bagbi, Y., Sarswat, A., Mohan, D., Pandey, A., & Solanki, P. R. (2016). Lead (Pb^{2+}) adsorption by monodispersed magnetite nanoparticles: Surface analysis and effects of solution chemistry. *Journal of Environmental Chemical Engineering*. *4*(4), 4237-4247. DOI: 10.1016/j.jece.2016.09.026.

Bajda, T., Szala, B., & Solecka, U. (2015). Removal of lead and phosphate ions from aqueous solutions by organo-smectite. *Environmental Technology*. *36*(22), 2872-2883. DOI: 10.1080/09593330.2015.1051135.

Blöcher, C., Dorda, J., Mavrov, V., Chmiel, H., Lazaridis, N. K., & Matis, K. A. (2003). Hybrid flotation—membrane filtration process for the removal of heavy metal ions from wastewater. *Water Research*. *37*(16), 4018-4026. DOI: 10.1016/s0043-1354(03)00314-2.

Dąbrowski, A., Hubicki, Z., Poskościelny, P., & Robens, E. (2004). Selective removal of the heavy metal ions from waters and industrial wastewaters by ion-exchange method. *Chemosphere*. *56*, 91-106. DOI: 10.1016/j.chemosphere.2004.03.006.

Duan, J., Liu, R., Chen, T., Zhang, B., & Liu, J. (2012). Halloysite nanotube-Fe_3O_4 composite for removal of methyl violet from aqueous solutions. *Desalination*. *293*, 46-52. DOI: 10.1016/j.desal.2012.02.022.

Dubinin, M. M. (1960). The Potential Theory of Adsorption of Gases and Vapors for Adsorbents with Energetically Nonuniform Surfaces. *Chemical Reviews*. *60*(2), 235-241. DOI: 10.1021/cr60204a006.

Ebrahim, S. E., Sulaymon, A. H., & Saad Alhares, H. (2015). Competitive removal of Cu^{2+}, Cd^{2+}, Zn^{2+}, and Ni^{2+} ions onto iron oxide nanoparticles from wastewater. *Desalination and Water Treatment*. *57*(44), 20915-20929. DOI: 10.1080/19443994.2015.1112310.

Elkamash, A., Zaki, A., & Elgeleel, M. (2005). Modeling batch kinetics and thermodynamics of zinc and cadmium ions removal from waste solutions using synthetic zeolite A. *Journal of Hazardous Materials*. *127*(1-3), 211-220. DOI: 10.1016/j.jhazmat.2005.07.021.

Freundlich, H. M. F. (1906). Uber die adsorption in losungen. *Zeitschrift für Physikalische Chemie*. *57A*, 385-470.

Fu, R., Wang, W., Han, R., & Chen, K. (2008). Preparation and characterization of γ-Fe_2O_3/ZnO composite particles. *Materials Letters*. *62*(25), 4066-4068. DOI: 10.1016/j.matlet.2008.05.006.

Ghasemi, E., Heydari, A., & Sillanpää, M. (2017). Superparamagnetic Fe_3O_4@EDTA nanoparticles as an efficient adsorbent for simultaneous removal of Ag(I), Hg(II), Mn(II), Zn(II), Pb(II) and Cd(II) from water and soil environmental samples. *Microchemical Journal*. *131*, 51-56. DOI: 10.1016/j.microc.2016.11.011.

Hashemian, S., Saffari, H., & Ragabion, S. (2014). Adsorption of Cobalt(II) from Aqueous Solutions by Fe_3O_4/Bentonite Nanocomposite. *Water, Air, & Soil Pollution*. *226*(1). DOI: 10.1007/s11270-014-2212-6.

Hosseinzadeh, M., Ebrahimi, S. A. S., Raygan, S., & Masoudpanah, S. M. (2016). Removal of Cadmium and Lead Ions from Aqueous Solution by Nanocrystalline Magnetite Through Mechanochemical Activation. *Journal of Ultrafine Grained and Nanostructured Materials*. *49*(2), 72-79. DOI: 10.7508.jufgnsm/2016.02.03.

Iyengar, S. J., Joy, M., Ghosh, C. H., Dey, S., Kotnala, R. K., & Ghosh, S. (2014). Magnetic, X-ray and Mössbauer studies on Magnetite/Maghemite Core-Shell Nanostructures Fabricated through Aqueous Route. *RSC Advances*. *4*(110), 64919-64929. DOI: 10.1039/b000000x.

Jiang, M.-q., Jin, X.-y., Lu, X.-Q., & Chen, Z.-l. (2010). Adsorption of Pb(II), Cd(II), Ni(II) and Cu(II) onto natural kaolinite clay. *Desalination*. *252*(1-3), 33-39. DOI: 10.1016/j.desal.2009.11.005.

Joussein, E., Petit, S., Churchman, J., Theng, B., Righi, D., & Delvaux, B. (2005). Halloysite clay minerals - a review. *Clay Minerals*. *40*, 383-426. DOI: 10.1180/0009855054040180.

Karimzadeh, I., Aghazadeh, M., Ganjali, M. R., Doroudi, T., & Kolivand, P. H. (2017). Preparation and characterization of iron oxide (Fe_3O_4) nanoparticles coated with polyvinylpyrrolidone/polyethylenimine through a facile one-pot deposition route. *Journal of Magnetism and Magnetic Materials*. *433*, 148-154. DOI: 10.1016/j.jmmm.2017.02.048.

Kharissova, O. V., Dias, H. V. R., & Kharisov, B. I. (2015). Magnetic adsorbents based on micro- and nano-structured materials. *RSC Adv.* *5*(9), 6695-6719. DOI: 10.1039/c4ra11423j.

Koteja, A., & Matusik, J. (2015). Di- and triethanolamine grafted kaolinites of different structural order as adsorbents of heavy metals. *Journal of Colloid and Interface Science*. *455*, 83-92. DOI: 10.1016/j.jcis.2015.05.027.

Kumari, M., Pittman, C. U., & Mohan, D. (2015). Heavy metals [chromium (VI) and lead (II)] removal from water using mesoporous magnetite (Fe_3O_4) nanospheres. *Journal of Colloid and Interface Science*. *442*, 120-132. DOI: 10.1016/j.jcis.2014.09.012.

Langmuir, I. (1916). The constitution and fundamental properties of solids and liquids. *Part I. Solids, J. Am. Chem. Soc*. *38*, 2221–2295. DOI: 10.1021/ja02254a006.

Lunge, S., Singh, S., & Sinha, A. (2014). Magnetic iron oxide (Fe_3O_4) nanoparticles from tea waste for arsenic removal. *Journal of Magnetism and Magnetic Materials*. *356*, 21-31. DOI: 10.1016/j.jmmm.2013.12.008.

Magnacca, G., Allera, A., Montoneri, E., Celi, L., Benito, D. E., Gagliardi, L. G., Gonzalez, M. C., Mártire, D. O., & Carlos, L. (2014). Novel Magnetite Nanoparticles Coated with Waste-Sourced Biobased Substances as Sustainable and Renewable Adsorbing Materials. *ACS Sustainable Chemistry & Engineering*. *2*(6), 1518-1524. DOI: 10.1021/sc500213j.

Matlock, M. M., Howerton, B. S., & Atwood, D. A. (2002). Chemical precipitation of heavy metals from acid mine drainage. *Water Research*. *36*, 4757-4764. DOI: 10.1016/S0043-1354(02)00149-5.

Matusik, J. (2010).Minerały z grupy kaolinitu jako prekursory nanorurek mineralnych (Kaolin group minerals as precursors of mineral nanotube). PhD thesis, AGH University of Science and Technology, Krakow, 174 pp. [in Polish].

Matusik, J. (2016). Halloysite for Adsorption and Pollution Remediation. In Yuan, Thill & Faiza, Nanosized Tubular Clay Minerals (606-627). Elsevier.

Matusik, J., & Wścisło, A. (2014). Enhanced heavy metal adsorption on functionalized nanotubular halloysite interlayer grafted with aminoalcohols. *Applied Clay Science*. *100*, 50-59. DOI: 10.1016/j.clay.2014.06.034.

Maziarz, P., & Matusik, J. (2016). The effect of acid activation and calcination of halloysite on the efficiency and selectivity of Pb(II), Cd(II), Zn(II) and As(V) uptake. *Clay Minerals*. *51*(3), 385-394. DOI: 10.1180/claymin.2016.051.3.06.

Mehta, D., Mazumdar, S., & Singh, S. K. (2015). Magnetic adsorbents for the treatment of water/wastewater–A review. *Journal of Water Process Engineering*. *7*, 244-265. DOI: 10.1016/j.jwpe.2015.07.001.

Motsi, T., Rowson, N. A., & Simmons, M. J. H. (2011). Kinetic studies of the removal of heavy metals from acid mine drainage by natural zeolite. *International Journal of Mineral Processing*. *101*(1-4), 42-49. DOI: 10.1016/j.minpro.2011.07.004.

Nightingale, E. R. (1959). Phenomenological theory of ion solvation. Effective radii of hydrated ions. *Journal of Physical Chemistry*. *63*, 1381-1387. DOI: 10.1021/j150579a011.

Oliveira, L. C. A., Rios, R. V. R. A., Fabris, J. D., Sapag, K., Garg, V. K., & Lago, R. M. (2003). Clay–iron oxide magnetic composites for the adsorption of contaminants in water. *Applied Clay Science*. *22*(4), 169-177. DOI: 10.1016/s0169-1317(02)00156-4.

Ozaki, H., Sharmab, K., & Saktaywirf, W. (2002). Performance of an ultra-low-pressure reverse osmosis membrane (ULPROM) for separating heavy metal: effects of interference parameters. *Desalination*. *144*, 287-294. DOI: 10.1016/S0011-9164(02)00329-6.

Papoulis, D., Komarneni, S., Nikolopoulou, A., Tsolis-Katagas, P., Panagiotaras, D., Kacandes, H. G., Zhang, P., Yin, S., Sato, T., & Katsuki, H. (2010). Palygorskite- and Halloysite-TiO2 nanocomposites: Synthesis and photocatalytic activity. *Applied Clay Science*. *50*(1), 118-124. DOI: 10.1016/j.clay.2010.07.013.

Rajput, S., Pittman, C. U., & Mohan, D. (2016). Magnetic magnetite (Fe_3O_4) nanoparticle synthesis and applications for lead (Pb^{2+}) and chromium (Cr^{6+}) removal from water. *Journal of Colloid and Interface Science*. *468*, 334-346. DOI: 10.1016/j.jcis.2015.12.008.

Rendon, J. L., & Serna, C. J. (1981). IR Spectra Of Powder Hematite: Effects Of Particle Size And Shape. *Clay Minerals*. *16*(4), 375-381.

Rodulfo-Baechler, S. M., González-Cortés, S. L., Orozco, J., Sagredo, V., Fontal, B., Mora, A. J., & Delgado, G. (2004). Characterization of modified iron catalysts by X-ray diffraction, infrared spectroscopy, magnetic susceptibility and thermogravimetric analysis. *Materials Letters*. *58*(20), 2447-2450. DOI: 10.1016/j.matlet.2004.02.032.

Rouxhet, P. G., Samudacheata, N., Jacobs, H., & Anton, O. (1977). Attribution Of The OH Stretching Bands Of Kaolinite. *Clay Minerals*. *12*, 171-179. DOI: 10.1180/claymin.1977.012.02.07

Rzepa, G., Bajda, T., & Ratajczak, T. (2009). Utilization of bog iron ores as sorbents of heavy metals. *Journal of Hazardous Materials*. *162*(2-3), 1007-1013. DOI: 10.1016/j.jhazmat.2008.05.135.

Silva, V. A. J., Andrade, P. L., Silva, M. P. C., Bustamante D, A., De Los Santos Valladares, L., & Albino Aguiar, J. (2013). Synthesis and characterization of Fe_3O_4 nanoparticles coated with fucan polysaccharides. *Journal of Magnetism and Magnetic Materials*. *343*, 138-143. DOI :10.1016/j.jmmm.2013.04.062.

Smičiklas, I. D., Milonjić, S. K., Pfendt, P., & Raičević, S. (2000). The point of zero charge and sorption of cadmium (II) and strontium (II) ions on synthetic hydroxyapatite. *Separation and Purification Technology*. *18*(3), 185-194. DOI: 10.1016/s1383-5866(99)00066-0.

Theng, B. K. G., Russel, M., Churchman, G. J., & Parfitt, R. L. (1982). Surface Properties Of Allophane, Halloysite, And Imogolite. *Clays and Clay Minerals*. *30*(2), 143-149. DOI: 10.1346/CCMN.1982.0300209.

Tian, X., Wang, W., Tian, N., Zhou, C., Yang, C., & Komarneni, S. (2016). Cr(VI) reduction and immobilization by novel carbonaceous modified magnetic Fe_3O_4/halloysite nanohybrid. *Journal of Hazardous Materials*. *309*, 151-156. DOI: 10.1016/j.jhazmat.2016.01.081.

Unuabonah, E. I., Adebowale, K. O., Olu-Owolabi, B. I., Yang, L. Z., & Kong, L. X. (2008). Adsorption of Pb (II) and Cd (II) from aqueous solutions onto sodium tetraborate-modified Kaolinite clay: Equilibrium and thermodynamic studies. *Hydrometallurgy*. *93*(1-2), 1-9. DOI: 10.1016/j.hydromet.2008.02.009.

Wang, C. Y., Hong, J. M., Chen, G., Zhang, Y., & Gu, N. (2010). Facile method to synthesize oleic acid-capped magnetite nanoparticles. *Chinese Chemical Letters*. *21*(2), 179-182. DOI: 10.1016/j.cclet.2009.10.024.

Wang, L., Cheng, C., Tapas, S., Lei, J., Matsuoka, M., Zhang, J., & Zhang, F. (2015). Carbon dots modified mesoporous organosilica as an adsorbent for the removal of 2,4- dichlorophenol and heavy metal ions. *Journal of Materials Chemistry A*. *3*, 13357-13364. DOI: 10.1039/c5ta01652e.

Wang, R., Jiang, G., Ding, Y., Wang, Y., Sun, X., Wang, X., & Chen, W. (2011). Photocatalytic Activity of Heterostructures Based on TiO2 and Halloysite Nanotubes. *ACS Applied Materials & Interfaces*. *3*(10), 4154-4158. DOI: 10.1021/am201020q.

Xie, Y., Qian, D., Wu, D., & Ma, X. (2011). Magnetic halloysite nanotubes/iron oxide composites for the adsorption of dyes. *Chemical Engineering Journal*. *168*(2), 959-963. DOI: 10.1016/j.cej.2011.02.031.

Xu, D., Tan, X., Chen, C., & Wang, X. (2008). Removal of Pb(II) from aqueous solution by oxidized multiwalled carbon nanotubes. *Journal of Hazardous Materials*. *154*(1-3), 407-416. DOI: 10.1016/j.jhazmat.2007.10.059.

Yantasee, W., Warner, C. L., Sangvanich, T., Addleman, R. S., Carter, T. G., Wiacek, R., Fryxell, G. E., Timchalk, C., & Warner, M. G. (2007). Removal of Heavy Metals from Aqueous Systems with Thiol Functionalized Superparamagnetic Nanoparticles. *Environmental Science & Technology*. *41*(14), 5114-5119. DOI: 10.1021/es0705238.

Zhang, S. Q., & Hou, W. G. (2008). Adsorption behavior of Pb(II) on montmorillonite. *Colloids and Surfaces A: Physicochemical and Engineering Aspects*. *320*(1-3), 92-97. DOI: 10.1016/j.colsurfa.2008.01.038.

Zhang, Z., & Kong, J. (2011). Novel magnetic Fe_3O_4@C nanoparticles as adsorbents for removal of organic dyes from aqueous solution. *Journal of Hazardous Materials*. *193*, 325-329. DOI: 10.1016/j.jhazmat.2011.07.033.